Article

# Catalytic Pt/Al$_2$O$_3$ Monolithic Foam for Ethanol Reforming Fabricated by the Competitive Impregnation Method

Mauro E. Silva Júnior,* Maíra O. Palm,* Diego A. Duarte,* and Rafael C. Catapan*

Read Online

ACCESS | Metrics & More | Article Recommendations | Supporting Information

**ABSTRACT:** Here, the synthesis of Pt/Al$_2$O$_3$ catalysts on a monolithic foam employing the competitive impregnation method is presented. NO$_3^-$ was used as a competitive adsorbate at different concentrations in order to delay the adsorption of Pt, minimizing the formation of Pt concentration gradients throughout the monolith. The catalysts' characterization includes the BET, H$_2$-pulse titration, SEM, XRD and XPS techniques. The catalytic activity evaluation was performed under partial oxidation and autothermal reforming of ethanol in a short contact time reactor. The competitive impregnation method was able to produce better dispersion of the Pt particles through the Al$_2$O$_3$ foams. XPS analysis indicated the catalytic activity of the samples, by the presence of metallic Pt and Pt oxides (PtO and PtO$_2$) in the internal regions of the monoliths. Compared to other Pt catalysts reported in the literature, the catalyst produced by the competitive impregnation method was revealed to be selective toward H$_2$. Overall, the results showed that the competitive impregnation method employing NO$_3^-$ as the co-adsorbate is a promising technique to synthesize well dispersed Pt catalysts over $\alpha$-Al$_2$O$_3$ foams.
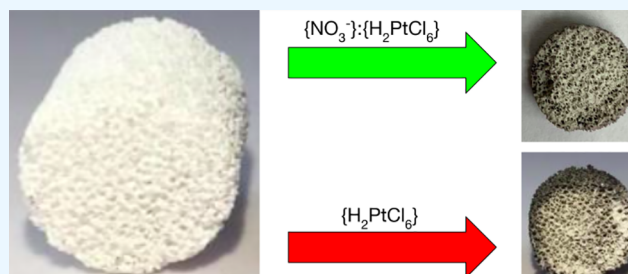
## ■ INTRODUCTION

Structured heterogeneous catalysts have been investigated for H$_2$ generation in embedded systems in short contact time reactors.[1−3] Such catalysts are usually supported on monoliths with a high surface area per unit volume ratio, promoting process intensification, while favoring a better flow distribution with lower pressure loss inside the reactor.[4,5] A substantial increase in the surface area of monoliths is achieved by covering them with a washcoat, improving the dispersion of the active phase of the metal and increasing the metallic area, which provides changes in both the reaction rate and the selectivity of the reactor.[6−9]

Catalysts with metallic active phases are often used in reforming reactions because they have a high capacity to cleave C−C bonds, an essential step for a high conversion of hydrocarbons into hydrogen.[10,11] Platinum (Pt) has great potential for use as an active phase in ethanol reforming, as it has high selectivity for H$_2$, activity at low temperatures and resistance to deactivation.[12−14] However, Pt is a very expensive metal when compared to other non-noble metals; thus, strategies to develop monoliths with highly dispersed structure catalysts are strongly desired.

The synthesis of well distributed metal particles on supports with complex geometries, e.g., foams, is a challenging task due to the rapid adsorption of metal complexes on the active sites, generating agglomerates and minimizing the surface area and activity, as reported for Pt catalysts[15−20] and Fe and Cu catalysts.[21] An alternative to improve the dispersion of Pt on the surface of Al$_2$O$_3$ foam, minimizing the formation of gradients of Pt through the monolith, is to use a competitive adsorbate during impregnation. The principle of this technique is based on adding a species that competes for the adsorption sites with the Pt complexes present in the impregnation solution.[18,22] This technique was employed for the synthesis of Pt/Al$_2$O$_3$ catalysts using organic acids as competitive adsorbates.[18] The authors obtained a decrease in particle size and an increase in the dispersion of Pt on the support. However, due to the high affinity of the adsorbates used by the surface of Al$_2$O$_3$, the increase in the competitor concentration can limit the properties of the synthesis due to the decrease in the adsorbed amount of active phase.

In this context, the present work aims at investigating the competitive impregnation method for the synthesis of Pt/Al$_2$O$_3$ on catalytic monoliths. NO$_3^-$ was used as a competitive adsorbate at different concentrations in order to delay the adsorption of Pt, allowing a better dispersion throughout the monolith. The catalysts synthesized by competitive adsorption had their properties compared to catalysts synthesized through the conventional methodology of wet impregnation. Scanning electron microscopy with a field emission gun (SEM-FEG), area measurement via BET and H$_2$-chemisorption under pulse
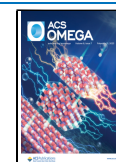
titration, X-ray diffraction (XRD) and X-ray photoelectron spectroscopy (XPS) were conducted to characterize the structure properties of the catalysts. The most promising catalysts had their catalytic activity and selectivity for $H_2$ evaluated in partial oxidation reactions and autothermal reforming of ethanol in a contact time reactor.

## ■ EXPERIMENTAL SECTION

**Catalyst Preparation.** Commercial foams of $\alpha$-$Al_2O_3$ (supplied by Goodfellow), with 26 pores/cm, 12.7 mm thick and 15 mm in diameter, were used as monoliths. Some samples went through the coating step, where the foams were submerged for 1 min in a slurry composed by 40 wt % of $\alpha$-$Al_2O_3$ (CT3000SG, supplied by Almatis, below 2.5 $\mu$m), 1 wt % of $HNO_3$ (Dinâmica, 65% analytical reagent), 1 wt % of sodium silicate (Dinâmica, analytical reagent) and 58 wt % of distilled water, prepared according to the methodology described in detail elsewhere.[9] Then, the foams were dried at 110 °C for 90 min, with a heating ramp of 3 °C/min to eliminate solvents and residues, and then calcined at 600 °C for 2 h at the rate of 6 °C/min. Both drying and calcination steps were carried out under a dry air flow with a flow rate of 50 cm$^3$/min. The coated supports went on to the impregnation stage, both conventional and competitive. In conventional impregnation, the active phase was impregnated onto the support using a $H_2PtCl_6 \cdot 6H_2O$ solution (supplied by Sigma-Aldrich, 99.9% purity). The foams were immersed in 4 mL of the precursor solution of 0.0257 molar concentration for 16 h, in order to obtain 1 wt % of Pt over the monolith. In the competitive impregnation, nitrate ($NO_3^-$) was used as a competing ion and added to the precursor solution of $H_2PtCl_6 \cdot 6H_2O$ via $HNO_3$. The $HNO_3$ concentration was calculated in order to obtain $[NO_3^-]$:$[H_2PtCl_6]$ ratios in the proportions of 10:1, 15:1 and 20:1. After conventional or competitive impregnation, the samples were dried for 12 h at 150 °C, with a heating ramp of 3 °C/min, and calcined for 2 h at 600 °C at a rate of 6 °C/min. Both drying and calcination steps were carried out under a flow of dry air, with a flow rate of 50 cm$^3$/min. A typical result of mass loss after impregnation was less than 1 wt % of the monolith, which is attributed to a problem of adhesion quality between the washcoat and monolith. Table 1 lists the main features of the monoliths.

**Table 1. Information on the Samples Produced, Including Coating Step, Metal Impregnation Method and Adsorbate Ratio**

| Sample | Impregnation method | $[NO_3^-]$:$[H_2PtCl_6]$ ratio |
|---|---|---|
| $Pt/Al_2O_3$ | Conventional | |
| $Pt/Al_2O_3$ R10 | Competitive | 10:1 |
| $Pt/Al_2O_3$ R15 | Competitive | 15:1 |
| $Pt/Al_2O_3$ R20 | Competitive | 20:1 |
| $Pt/Al_2O_3$-coated | Conventional | |
| $Pt/Al_2O_3$ R10-coated | Competitive | 10:1 |
| $Pt/Al_2O_3$ R20-coated | Competitive | 20:1 |

**Catalyst Characterization.** Fragments (0.15−0.2 g) from different regions of the foam were analyzed by scanning electron microscopy with a field emission gun (SEM-FEG) in a high-resolution microscope (JSM-6701F by JEOL). Prior to the analysis, the specimen was sputter-coated with gold to avoid charge accumulations. The Brunauer−Emmett−Teller (BET) area and the metal surface area were measured in a ChemBET pulsar TPR/TPD analyzer (by Quantachrome). The $H_2$-pulse

titration (PT) technique was performed to determine the metal surface area, particle diameter and metal dispersion. Details on the procedures are presented elsewhere.[9]

The X-ray diffraction technique (XRD) was used to study the crystalline structure of the synthesized monoliths, using the PANalytical Empyrean equipment with a copper target (Cu K$\alpha$ radiation 1.5418 Å), 40 kV and 40 mA, angle of $20° < 2\theta < 110°$ and scan speed of 0.09°/s. The identification of the phases in the diffractions was carried out with the aid of the HighScore software by comparison with the database of the International Center for Diffraction Data (ICDD). In this technique, the crystallite average sizes ($d_p$) were calculated using the Scherrer equation:

$$d_p = \frac{(0.89)\lambda}{\beta \cos(\theta)} \tag{1}$$

where $\lambda$ is the X-ray wavelength (1.5406 Å for Cu K$\alpha$), $\theta$ is the diffraction angle, and $\beta$ is the full peak width at half-maximum.

X-ray excited photoelectron spectroscopy (XPS) analyzes were performed using the Scienta-Omicron ESCA model spectrometer. Survey spectra were obtained between zero and 1200.00 eV with a step of 0.50 eV and 100 ms dwell time per sweep. High-resolution spectra were measured for the Pt 4f, Al 2p, O 1s and C 1s states produced from the average of 3 sweeps obtained with a step of 0.05 eV and 200 ms dwell time per sweep. Pass energy, spot size aperture and exit slit were kept at 50.00 eV, 5 and 5 × 11 mm, respectively. Spectra were collected in the CAE mode. All spectra were obtained with a flood gun. Before or during the analysis, sputtering with an ion gun was not performed. The X-rays were produced with the aluminum K$\alpha$ line (1486.6 eV). The data were analyzed by the nonlinear least-squares technique assuming that the spectra can be approximated with a combination of Gaussian and Lorentzian curves, with the aid of the XPSPEAK41 program. Due to the characteristic asymmetry of the platinum peaks, the Pt 4f spectra were fitted with a 20% Lorentzian contribution. The spectra of the other elements were adjusted with 100% Gaussian contribution. The background was removed using Shirley's method. Alignment of the spectra was performed with the procedures described in ref 23 assuming that the surface work function is defined mainly by platinum, whose value is 5.7 eV.[24] The signals from the Pt 4f and Al 2p spectra are superimposed. Thus, the separation distance and the ratio between the intensities ($I_{7/2}/I_{5/2}$) of the Pt 4f$_{7/2}$ and Pt 4f$_{5/2}$ peaks in all detected Pt$^0$, Pt$^{2+}$ and Pt$^{4+}$ states were set at 3.3 eV and 0.75, respectively, to minimize errors in the detection of platinum states.[25] The chemical composition was calculated considering the following atomic sensitivity factors (ASFs): 0.193 (Al 2p), 0.296 (C 1s), 0.711 (O 1s) and 4.674 (Pt 4f).[26]

**Catalytic Reactions.** The experimental apparatus used to evaluate the catalytic activity of the monoliths was presented in detail elsewhere.[9] For each run, one catalytic monolith was placed inside a quartz tube between two fresh $Al_2O_3$ foams to homogenize the inlet flow of reactants. The quartz tube was placed inside a temperature-controlled furnace. Gas sampling employs a volumetric flask to cool down byproducts before being sent to the gas chromatograph (GC) (Clarus 580 by PerkinElmer) equipped with a sampling loop of 2 mL. The GC was equipped with a thermal conductivity detector, which detects $H_2$, $O_2$, and $N_2$, and a flame ionization detector, which detects the organic species. Because of the high uncertainties, water was not considered in the molar fraction of the products.
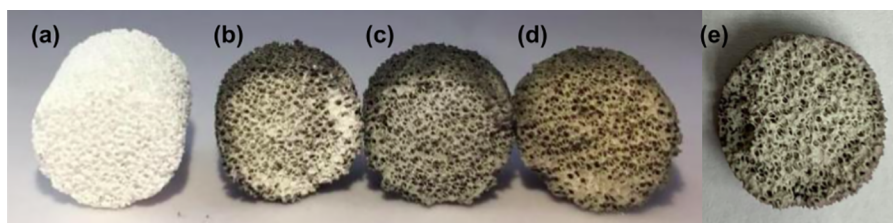
**Figure 1.** Images of the samples uncoated and without impregnation of the active phase (a), $Pt/Al_2O_3$-coated (b), $Pt/Al_2O_3$ R10 (c), $Pt/Al_2O_3$ R20 (d) and $Pt/Al_2O_3$ R20-coated (e). Sample (b) was prepared with the conventional method. Samples (c), (d) and (e) were prepared with the competitive adsorption method. Sample details are as described in Table 1.
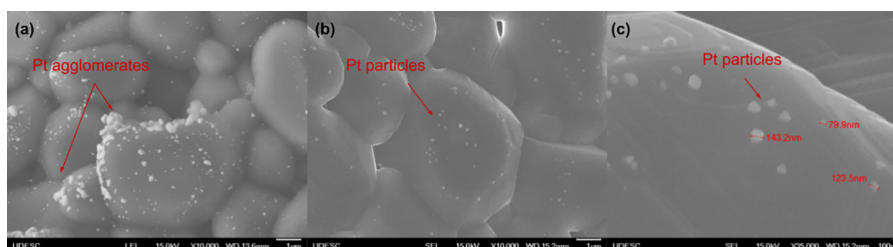


**Figure 2.** SEM images of the $Pt/Al_2O_3$ sample at: (a) external region with magnification of 10,000×; (b) internal region with magnification of 10,000× and (c) internal region with magnification of 35,000×, showing the contrast between agglomeration of the active phase externally and particles sparsely distributed internally in the monolith.
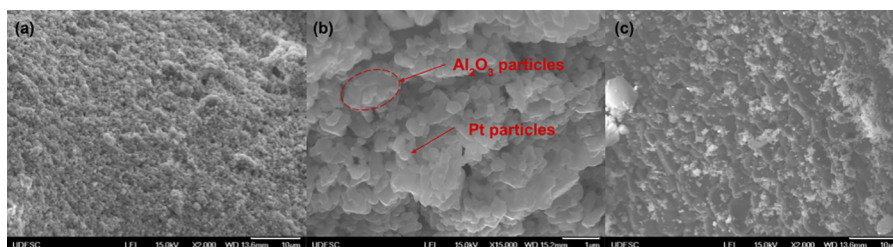


**Figure 3.** SEM images of the $Pt/Al_2O_3$-coated sample at: (a) external region with magnification of 2,000×; (b) external region with magnification of 15,000× and (c) internal region with magnification of 2,000×, evidencing agglomeration of the active phase externally on the monolith.

The columns Rt-U-BOND e Elite GC GS-Molesieve, 30 m long and 0.53 mm of internal diameter (by Restek), were used. Quantitative calibration was performed using samples from the species that were to be detected in the tests. Ar (99.999% pure) was used as the carrier gas.

Autothermal reforming (ATR) and partial oxidation (POX) of ethanol were carried out under stoichiometric conditions. Both water and ethanol were added in the reactions by a saturator maintained at around 70 °C. The saturator employed $N_2$ (99.9% purity) with a flow of 1 L/min, controlled by an electronic flow controller (by Alicat) as the carrier gas. The concentration of ethanol entering the reactor was measured by GC analysis before each test. The flow rates of the remaining reagents were adjusted in order to obtain the required ratio to ethanol for each test.

A typical run consisted of reducing Pt catalyst under a 5% $H_2/N_2$ flow for 1 h and 500 °C. Subsequently, the furnace was set to the desired temperature and the reactor was kept under a flow of 5 L/min of $N_2$ for 20 min before feeding the reactants. Reactions were diluted with 98% of $N_2$ in order to reduce the temperature gradients while maintaining approximately the same total flow rate of 5 L/min and consequently the same residence time of 27 ms. After 3 min of reaction, a 2 mL gas sample was sent to the GC with the aid of a sampling loop. After each test, the catalyst was regenerated by flowing 100 cm³/min of air at 500 °C for 1 h. The product selectivity was defined as the ratio of moles of one

product by the total moles of products, excluding the reactants $C_2H_5OH$, $O_2$ and $H_2O$. The activity and selectivities of the catalysts were evaluated at temperatures of 450 to 650 °C. The largest errors in the carbon balance (between reactor inlet and outlet) were approximately 11% for partial oxidation and 16% for steam reforming reactions, respectively, reported elsewhere for the same experimental apparatus.[9]

## ■ RESULTS AND DISCUSSION

**Catalysts' Characterization.** *Visual Inspection and SEM Images.* Figure 1 shows images of the samples uncoated and without impregnation of the active phase (a), $Pt/Al_2O_3$-coated impregnated by the conventional method (b), $Pt/Al_2O_3$ R10 (c), $Pt/Al_2O_3$ R20 (d) and $Pt/Al_2O_3$ R20-coated impregnated by the competitive impregnation method (e). Visual inspection indicates a gray color gradient over the $Pt/Al_2O_3$-coated sample, impregnated by the conventional method (Figure 1b). This result suggests that a Pt concentration gradient was formed across the monolith.[27] These concentration gradients, also called egg shell, are undesirable for catalytic reactions since they decrease the surface area and consequently the catalytic activity.[13]

Figures 1c, 1d and 1e show the catalytic monoliths prepared by competitive impregnation with and without coating and for different competitive adsorbate ratios. In comparison with the samples made by the conventional method, the catalysts

prepared by competitive adsorption were more homogeneous and had a less intense gray tone, with no visible color gradient. The lower gray intensity is attributed to the effect of the lower Pt surface concentration,[28] suggesting a better dispersion of the Pt content through the monolith. These results suggest that the synthesis by competitive impregnation provided a more homogeneous impregnation of the active phase of the catalyst.

The presence of metal agglomerations over the external surfaces of the monolith fabricated by the conventional method is corroborated by the analysis of the SEM images. Figure 2a presents the SEM image at the external region of the Pt/Al₂O₃ sample, indicating agglomeration of the active phase. In contrast, Figures 2b and 2c indicate Pt particles, in the order of 70 to 150 nm, sparsely distributed over the monolith. Figures 3a and 3b show SEM images of the external regions of the Pt/Al₂O₃-coated sample, indicating a more intense agglomeration of the active phase due to the presence of the coating layer with alumina particles (between 0.5 and 2.5 μm). Smaller particles are attributed to the Pt. Figure 3c shows a SEM image of the sample internal region in the Pt/Al₂O₃-coated sample, indicating fewer and sparsely distributed particles.

*XPS Analysis.* Figure 4 shows the spectrum of the Pt 4f orbital of the Pt/Al₂O₃-coated sample, which has the same behavior as
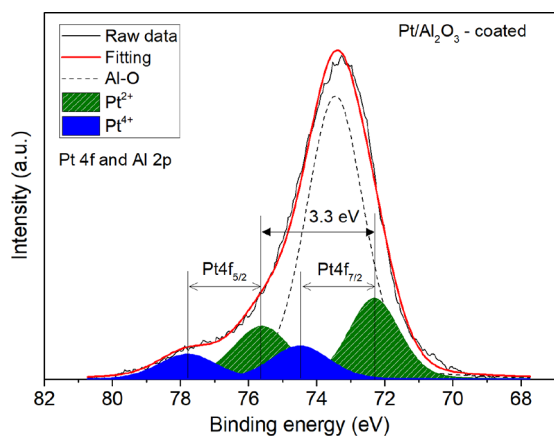


**Figure 4.** XPS spectrum corresponding to the Pt 4f and Al 2p levels of the Pt/Al₂O₃-coated sample.

the spectra of the Pt/Al₂O₃ R10-coated and Pt/Al₂O₃ R20-coated samples (see Supporting Information). The strongest signal is related to the presence of the Al−O bond of alumina located at 73.4 ± 0.1 eV. The other signals refer to the $Pt^{2+}$ (PtO) and $Pt^{4+}$ (PtO₂) states located at 72.3 ± 0.1 eV and 74.4 ± 0.1 eV, respectively.[25] The estimated percentages of Pt in the Pt/Al₂O₃-coated, Pt/Al₂O₃ R10-coated and Pt/Al₂O₃ R20-coated samples, considering the signals of levels Pt 4f, Al 2p, O 1s and C 1s, are around 1.1, 1.8 and 0.9%, respectively. These values are approximations, considering the complexity of the overlapping of the Pt 4f and Al 2p spectra, which makes it difficult to determine the exact intensity of the platinum signals, and the lack of precision of the ASFs for the equipment used. The correct position of the peaks is also imprecise due to the lack of the real value of the work function of the surfaces. The three samples show no sign of metallic Pt.

Figure 5 shows the spectrum of the Pt 4f orbital of Pt/Al₂O₃ R10 sample, which has a similar behavior to the spectrum of the Pt/Al₂O₃ R20 sample. The strongest signal is related to the presence of the Al−O bond of alumina located at 73.2 ± 0.2 eV. The other signals refer to the $Pt^0$ (Pt), $Pt^{2+}$ (PtO) and $Pt^{4+}$
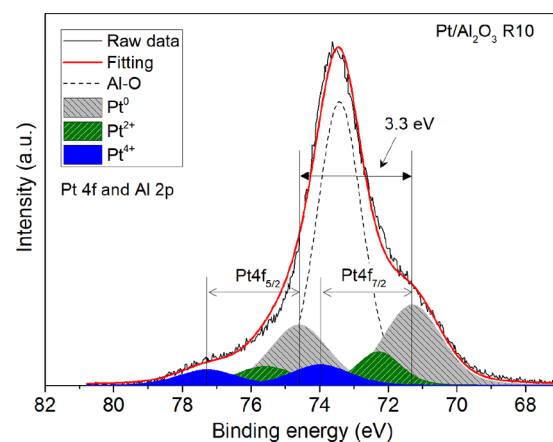


**Figure 5.** XPS spectrum corresponding to the Pt 4f and Al 2p levels of the Pt/Al₂O₃ R10 sample.

(PtO₂) states located at 70.8 ± 0.5 eV, 72.3 eV and 73.8 ± 0.2 eV, respectively.[25] The estimated percentages of Pt in samples Pt/Al₂O₃ R10 and Pt/Al₂O₃ R20 are around 0.6 and 2.8%, respectively. As mentioned before, their values have to be taken carefully due to the imprecision in the position of the peaks. Samples Pt/Al₂O₃ R10 and Pt/Al₂O₃ R20 show metallic platinum signal. The spectrum of the Pt 4f level of the Pt/Al₂O₃ R20 sample is shown in the Supporting Information. The results show an unknown peak at 75.5 eV that may be related to the formation of aluminum hydroxide or sub-oxide.[29,30]

*XRD Diffraction Patterns.* Figure 6 presents the diffracto-grams for the catalysts made by both conventional and
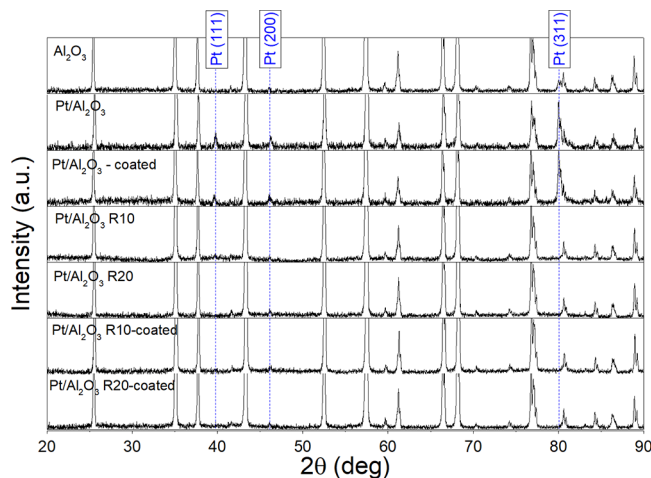


**Figure 6.** Diffractograms of α-Al₂O₃ and the different Pt/Al₂O₃ catalyst samples. Sample details are as described in Table 1.

competitive impregnation. Pt crystal peaks are observed in Pt/Al₂O₃ and Pt/Al₂O₃-coated samples, prepared by conventional impregnation, at 2θ = 39.8°, 46.3° and 80° in good agreement with the (111), (200) and (311) Pt crystal planes reported by refs 31−33. On the other hand, in the samples produced by competitive impregnation, a small Pt crystal peak was observed at 46.3°, presenting spectra similar to the spectrum of the Al₂O₃ support. The absence of Pt signals in the samples produced by the competitive methodology also suggests better particle dispersion, leading to lower particle size. Similar XRD results were observed for Pt/Al₂O₃ catalysts,[34] for Pt/Al₂O₃-CeO₂ catalysts[35] and for Co/Al₂O₃ catalysts promoted by Pt.[36]

Aluminum oxide (ICDD 00-011-0661) with rhombohedral crystal structure and $R\overline{3}c$ space group was identified for both catalysts, being attributed to $Al_2O_3$.

*BET and H$_2$-Pulse Titration Analysis.* Table 2 presents the results of metallic area ($S_M$), particle diameter ($d_p$) and

**Table 2. Metallic Area ($S_M$), Particle Diameter ($d_p$) and Dispersion ($D$) for different Pt/Al$_2$O$_3$ Catalyst Samples.**

| Sample | $S_M$ (m$^2$/g) | $d_p$ (nm) | $D$ (%) |
|---|---|---|---|
| Pt/Al$_2$O$_3$ | | 58.91[a] | |
| Pt/Al$_2$O$_3$-coated | | 49.13[a] | |
| Pt/Al$_2$O$_3$ R10 | 0.09 | 7.54[b] | 3.75 |
| Pt/Al$_2$O$_3$ R15 | 0.10 | 7.16[b] | 3.96 |
| Pt/Al$_2$O$_3$ R20 | 0.11 | 6.31[b] | 4.49 |
| Pt/Al$_2$O$_3$ R10-coated | 0.10 | 6.72[b] | 4.21 |
| Pt/Al$_2$O$_3$ R20-coated | 0.14 | 5.07[b] | 5.58 |

[a]From DRX analysis. [b]From H$_2$-pulse titration analysis.

dispersion ($D$) for catalysts prepared by conventional and competitive impregnation. Particle sizes measured by XRD in the conventional method (Pt/Al$_2$O$_3$ and Pt/Al$_2$O$_3$-coated samples) were in the order of 50 to 60 nm. SEM results identified particles a little bigger, as observed in Figure 2. The competitive impregnation method produced smaller particle sizes than the conventional method, indicated by the measurements from the H$_2$-pulse titration, corroborating the hypothesis of greater metallic dispersion provided by the method. Despite the difference in the technique used for particle size measurement, the comparison remains valid, since in general, the XRD analysis applying the Scherrer equation (eq 1) indicates smaller particle diameters than applying the H$_2$-pulse titration analysis for the same catalyst.[37] The increase in the concentration of competitive adsorbate (R10 to R20) has caused a small reduction in the particle diameter, associated with the effect of competition for adsorption between Pt and $NO_3^-$. This is in a good agreement with the results reported by Zhang et al.[18] for the synthesis of Pt/Al$_2$O$_3$ catalysts employing lactic, maleic and oxalic acids as competitive adsorbates. The addition of these adsorbates increased the dispersion of Pt on the support, with a consequent reduction in the particle diameter. However, the strong interaction of these acids with Al$_2$O$_3$ reduced the amount of Pt adsorbed, a fact that impeded the synthesis of catalysts with the desired metal content.[18] Due to its weaker interaction with the support, $NO_3^-$ improves the characteristics of the metallic phase and does not make difficult the adsorption of the desired amount of Pt, due to the greater affinity of Pt complexes for the support. However, longer impregnation times and higher competitive adsorbate ratios are required.[28,38] BET analyses of the monolith were performed before and after the coating step, revealing an increase in surface area about 7.8 times after coating. The surface area of the uncoated monolith was 0.16 m$^2$/g, and after coating (Pt/Al$_2$O$_3$-coated sample) a surface area of 1.25 m$^2$/g was achieved. The greater number of active sites for adsorption of platinum complexes evidenced the phenomenon of concentration gradients.[39]

**Activity for Partial Oxidation and Autothermal Reforming of Ethanol.** Blank experiments employing the α-Al$_2$O$_3$ sample revealed ethanol conversions in the POX reaction below 3% at 440 °C and below 17% at 540 °C.[9] Product selectivity were mostly toward C$_2$H$_4$O and H$_2$, suggesting that part of the dehydrogenating reaction takes place over the α-Al$_2$O$_3$ support. On the other hand, selectivity toward C1

products, e.g., CO and CH$_4$, was lower than 5% at 540 °C, revealing no ability of the support to break the ethanol C−C bond. Figure 7 shows the ethanol conversions for the POX and
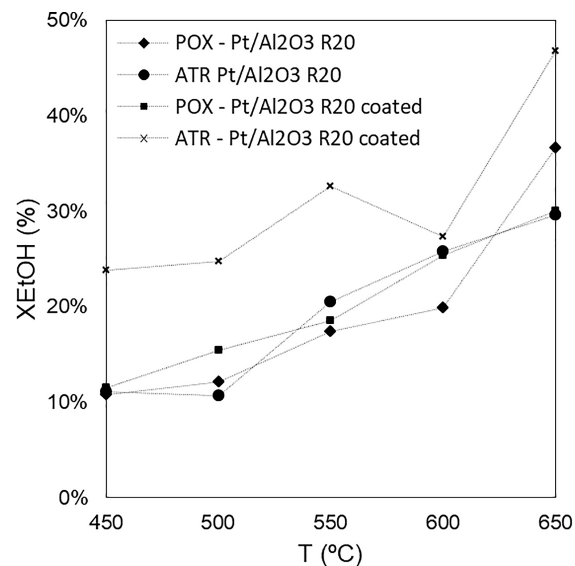
**Figure 7.** Conversion of ethanol over the Pt/Al$_2$O$_3$ R20 and Pt/Al$_2$O$_3$ R20-coated catalysts, with a space time of 27 ms.

ATR reactions over the Pt/Al$_2$O$_3$ R20 and Pt/Al$_2$O$_3$ R20-coated catalysts. In general, and as expected, conversions increase with temperature in all Pt catalysts and reactions. Additionally, the conversions are higher in both reactions on the Pt/Al$_2$O$_3$ R20-coated sample. The highest ethanol conversions were obtained for ATR reaction aided by the presence of O$_2$ and H$_2$O, simultaneously, over a catalyst with a higher active area. Overall, the low levels of ethanol conversion on both reactions are related to the very low residence time, in order of 27 ms, and low catalyst concentrations.

Product selectivities in the POX and ATR reactions over Pt/Al$_2$O$_3$ R20 and Pt/Al$_2$O$_3$ R20-coated catalysts are shown in the Supporting Information. Overall, the main product in both POX and ATR reactions over Pt/Al$_2$O$_3$ R20 is C$_2$H$_4$O, followed by H$_2$ and CO$_2$, suggesting that the presence of O$_2$ favors the oxidation of CO, CH$_4$ and H$_2$. On the other hand, the effectiveness of the C$_2$H$_4$O decomposition reaction increases in the Pt/Al$_2$O$_3$ R20-coated catalyst, decreasing the C$_2$H$_4$O while increasing the selectivity toward H$_2$ and CO$_2$. The formation of C$_2$H$_4$O in the ethanol reactions under short spatial time was already reported,[40] suggesting that high spatial velocities make difficult the rupture of the C−C bonds of the ethanol.

**Hydrogen Selectivity.** Table 3 compares the selectivity toward H$_2$ measured in the present work with values reported in the literature for several catalytic systems.[12,41−43] The POX reaction presented lower H$_2$ selectivity, probably due to the H$_2$ oxidation to H$_2$O. The presence of H$_2$O in the reactants of the ATR reaction increased H$_2$ selectivity. Despite the differences in the definition of selectivity in the literature, the Pt/Al$_2$O$_3$ catalysts employed in this study obtained promising results, especially after the coating, e.g., 35% and 48% in the POX and ATR reactions, respectively.

**Mechanism of the Competitive Adsorption between Pt and NO$_3^-$ over Al$_2$O$_3$.** The Pt coverage gradient over the monolith (see Figure 1) is due to the rapid adsorption of Pt complexes on the Al$_2$O$_3$ surface. According to Bel'skaya and

**Table 3. Selectivity toward H$_2$ for Different Pt/Al$_2$O$_3$ Catalyst Samples in Comparison with Values Found in the Literature for Thanol Reforming Reactions**

| Catalyst | Reaction | $T$ (°C) | $S_{H_2}$ (%) | Reference |
|---|---|---|---|---|
| 5% Pt/Al$_2$O$_3$ | POX | 900 | 50[a] | 41 |
| 1% Pt/Al$_2$O$_3$ | SR | 850 | 80[b] | 42 |
| 0.2% Pt/Al$_2$O$_3$ | SR | 600 | 55[a] | 12 |
| 0.2% Rh/Al$_2$O$_3$ | SR | 500 | 63[a] | 12 |
| 1.6% Rh/Al$_2$O$_3$ | ATR | 600 | 94[c] | 43 |
| 1.5% Pt/Al$_2$O$_3$ | ATR | 600 | 29[c] | 43 |
| 1% Pt/Al$_2$O$_3$ R20 | POX | 650 | 18[a] | This work |
| 1% Pt/Al$_2$O$_3$ R20 | ATR | 650 | 28[a] | This work |
| 1% Pt/Al$_2$O$_3$ R20-coated | POX | 650 | 35[a] | This work |
| 1% Pt/Al$_2$O$_3$ R20-coated | ATR | 650 | 48[a] | This work |

[a]Calculated as the ratio between moles of H$_2$ over the total moles of products, excluding any C$_2$H$_5$OH, H$_2$O and O$_2$. [b]Calculated as the ratio between moles of H$_2$ over the moles of C$_2$H$_5$OH consumed in the reaction. [c]Calculated as the ratio between moles of H$_2$ in the specific product over the total moles over H$_2$ in the products.

**Table 4. Mechanism of the Competitive Adsorption between Pt and NO$_3^-$ over Al$_2$O$_3$[a]**

| Reaction steps | |
|---|---|
| $S-OH + H+ \rightleftharpoons S-OH_2^+$ | R.01 |
| $[PtCl_6]^{2-} + 2S-OH_2^+ \rightleftharpoons [2S-OH_2]^{2+}[PtCl_6]^{2-}$ | R.02 |
| $[PtCl_6]^{2-} + H_2O \rightleftharpoons [PtCl_5(H_2O)]^- + Cl^-$ | R.03 |
| $[PtCl_5(H_2O)]^- + S-OH_2^+ \rightleftharpoons [S-OH_2]^+[PtCl_5(H_2O)]^-$ | R.04 |
| $S-OH_2^+ + Cl^- \rightleftharpoons [SOH_2]^+Cl^-$ | R.05 |
| $S-OH + [PtCl_6]^{2-} \rightleftharpoons S-[(OH)PtCl_5]^- + Cl^-$ | R.06 |
| $S-OH + [PtCl_5(H_2O)]^- \rightleftharpoons S-[(OH)PtCl_4(H_2O)]^0 + Cl^-$ | R.07 |
| $S-OH + [PtCl_6]^{2-} + H^+ \rightleftharpoons S-[(Cl)PtCl_5]^- + H_2O$ | R.08 |
| $S-OH + [PtCl_5(H_2O)]^- + H^+ \rightleftharpoons S-[(Cl)PtCl_4(H_2O)]^0 + H_2O$ | R.09 |
| $S-OH_2^+ + NO_3^- \rightleftharpoons [S-OH_2]^+NO_3^-$ | R.10 |
| $[2S-OH_2]^{2+}[PtCl_6]^{2-} + 2NO_3^- \rightleftharpoons [2S-OH_2]^{2+}[2NO_3]^{2-} + [PtCl_6]^{2-}$ | R.11 |
| $[S-OH_2]^+[PtCl_5(H_2O)]^- + NO_3^- \rightleftharpoons [S-OH_2]^+NO_3^- + [PtCl_5(H_2O)]^-$ | R.12 |
| $[S-OH_2]^+Cl^- + NO_3^- \rightleftharpoons [S-OH_2]^+NO_3^- + Cl^-$ | R.13 |

[a]S stands for the support surface atoms, Al$_3^+$.

Duplyakin,[38] there are two distinct mechanisms for the adsorption of Pt complexes over Al$_2$O$_3$. The first mechanism is by electrostatic attraction between the surface and the complex, while the second deals with chemical adsorption reactions, with exchange of ligands between the complexes and the active sites of the support. The nature of the Pt complexes present in the impregnation solution can be altered by aquation and hydrolysis reactions between PtCl$_6^{2-}$ species and H$_2$O. Since hydrolysis of platinum chloride complexes is strongly accelerated by temperatures higher than 80 °C,[38] thus temperature may affect the mechanism of Pt adsorption and potentially the efficiency of the process. However, under conditions where the impregnation is carried out without contact with light and ambient temperature, the occurrence of hydrolysis and aquation reactions can be attenuated. In this work, the pH of the impregnation solutions performed was below 2.5. Thus, the predominant mechanism for the adsorption of the Pt complexes is electrostatic attraction.[38] In conventional impregnation, this phenomenon of electrostatic attraction causes the active phase to be primarily retained on the external pores of the catalyst, without time for the complexes to diffuse through the pores, finding the internal sites.[16,22] The reactions R.01 to R.09 in Table 4 represent the adsorption mechanism of Pt complexes on Al$_2$O$_3$, under the conditions of the study. The reactions R.10 to R.13 are those involved when NO$_3^-$ is added to the impregnation step (S stands for the support surface atoms, Al$_3^+$).[28,38]

The OH radicals bind to the surface by the decomposition of water and are subsequently protonated via R.01, forming the active sites for adsorption. R.02 and R.04 are the reactions of the electrostatic mechanism. The R.03 reaction takes place on a smaller scale under the experimental conditions used, but it can be accelerated in contact with light or by increasing the temperature of the precursor solution.[38] The reactions R.06 to R.09 belong to the ligand exchange mechanism, and they occur more effectively with increasing pH.[44] Due to the physical nature of the mechanism, decreasing the pH of the impregnation solution increases the interaction between the complexes and the surface.

The addition of NO$_3^-$ causes the S–OH$_2^+$ sites to be disputed by the competitive adsorption with Pt. Shyr and Ernst[28] performed impregnation experiments with addition of NO$_3^-$ in

the ratio of 1.77, varying the impregnation time in 1 and 22 h. The results suggested that the reactions R.02 and R.04 happened faster and that the interaction between the Pt complexes and Al$_2$O$_3$ is stronger, with the egg shell concentration profile obtained in the catalysts after 1 h. After 22 h of impregnation, the concentration profile in the catalysts had a slight change, with an improvement in the concentration gradient, suggesting that NO$_3^-$ can participate in ion exchange reactions with the already adsorbed Pt complexes, causing the complex to return to liquid phase and diffuse to the internal pores of the support (reactions R.11 and R.12).

## ◾ CONCLUSIONS

The synthesis of well dispersed Pt/Al$_2$O$_3$ catalytic monoliths was investigated employing the competitive impregnation method. NO$_3^-$ was used as a competitive adsorbate at different concentrations in order to delay the adsorption of Pt. The addition of NO$_3^-$ in the precursor solution minimized the formation of Pt coverage gradients on the support and, consequently, provided a better dispersion of the active phase, reducing regions of Pt agglomerations. XPS analysis indicates the catalytic activity of the coated and uncoated samples prepared by the competitive impregnation method, by the presence of metallic Pt and Pt oxides (PtO and PtO$_2$) in the internal regions of the monoliths. Also, the results indicate the percentage of Pt over the support in the order of 1 to 2% of the surface, indicating the dispersion of the metallic phase through the entire monolith. The catalytic evaluation of the Pt/Al$_2$O$_3$ R20 and Pt/Al$_2$O$_3$ R20-coated catalysts revealed the presence of C$_2$H$_4$O, CO$_2$ and H$_2$, due to the very short contact time employed, around 27 ms. Compared to other Pt catalysts reported in the literature, the Pt/Al$_2$O$_3$ R20-coated catalyst was revealed to be selective toward H$_2$ under the ATR reaction. The fabrication of catalytic monoliths based on not only Pt, but other metals as well, can be positively affected by the results reported here. Overall, the results showed that the competitive impregnation method employing NO$_3^-$ is a promising technique to synthesize well dispersed Pt catalysts over α-Al$_2$O$_3$ monoliths.

## ■ ASSOCIATED CONTENT

**Ⓢ Supporting Information**

The Supporting Information is available free of charge at https://pubs.acs.org/doi/10.1021/acsomega.2c06870.

XPS spectrum of the Pt/Al$_2$O$_3$ R10-coated and Pt/Al$_2$O$_3$ R20-coated samples and product selectivities in the POX and ATR reactions over Pt/Al$_2$O$_3$ R20 and Pt/Al$_2$O$_3$ R20-coated samples (PDF)

## ■ AUTHOR INFORMATION

**Corresponding Authors**

**Mauro E. Silva Júnior** − *Laboratory of Applied Catalysis, Joinville Center of Technology, Federal University of Santa Catarina, 89219-600 Joinville, SC, Brazil;* Email: maurojunior270@gmail.com

**Maíra O. Palm** − *Laboratory of Applied Catalysis, Joinville Center of Technology, Federal University of Santa Catarina, 89219-600 Joinville, SC, Brazil;* Email: maira.o.palm@gmail.com

**Diego A. Duarte** − *Laboratory of Surface Treatments, Joinville Center of Technology, Federal University of Santa Catarina, 89219-600 Joinville, SC, Brazil;* Email: diego.duarte@ufsc.br

**Rafael C. Catapan** − *Laboratory of Applied Catalysis, Joinville Center of Technology, Federal University of Santa Catarina, 89219-600 Joinville, SC, Brazil;* ⓞ orcid.org/0000-0003-3052-7631; Email: rafael.catapan@ufsc.br

Complete contact information is available at:
https://pubs.acs.org/10.1021/acsomega.2c06870

**Notes**

The authors declare no competing financial interest.

## ■ ACKNOWLEDGMENTS

## ■ REFERENCES

(1) Ambroise, E.; Courson, C.; Roger, A.-C.; Kiennemann, A.; Blanchard, G.; Rousseau, S.; Carrier, X.; Marceau, E.; La Fontaine, C.; Villain, F. Exhaust gas recirculation for on-board hydrogen production by isooctane reforming: Comparison of performances of metal/ceria−zirconia based catalysts prepared through pseudo sol−gel or impregnation methods. *Catal. Today* **2010**, *154*, 133−141.

(2) Brookshear, D. W.; Pihl, J. A.; Szybist, J. P. Catalytic Steam and Partial Oxidation Reforming of Liquid Fuels for Application in Improving the Efficiency of Internal Combustion Engines. *Energy Fuels* **2018**, *32*, 2267−2281.

(3) Sawatmongkhon, B.; Theinnoi, K.; Wongchang, T.; Haoharn, C.; Wongkhorsub, C.; Sukjit, E. Modeling of Hydrogen Production from Catalytic Partial Oxidation of Ethanol over a Platinum−Rhodium-Supported Catalyst. *Energy Fuels* **2021**, *35*, 4404−4417.

(4) Faure, R.; Rossignol, F.; Chartier, T.; Bonhomme, C.; Maître, A.; Etchegoyen, G.; Del Gallo, P.; Gary, D. Alumina foam catalyst supports for industrial steam reforming processes. *J. Eur. Ceram. Soc.* **2011**, *31*, 303−312.

(5) Claude, V.; Mahy, J. G.; Lohay, T.; Geens, J.; Lambert, S. D. Coating Process of Honeycomb Cordierite Support with Ni/Boehmite Gels. *Processes* **2022**, *10*, 875.

(6) Degenstein, N.; Subramanian, R.; Schmidt, L. Partial oxidation of n-hexadecane at short contact times: Catalyst and washcoat loading and catalyst morphology. *Appl. Catal., A* **2006**, *305*, 146−159.

(7) Fernández, A.; Arzac, G.; Vogt, U.; Hosoglu, F.; Borgschulte, A.; de Haro, M. J.; Montes, O.; Züttel, A. Investigation of a Pt containing washcoat on SiC foam for hydrogen combustion applications. *Appl. Catal., B* **2016**, *180*, 336−343.

(8) Gao, N.; Liu, S.; Han, Y.; Xing, C.; Li, A. Steam reforming of biomass tar for hydrogen production over NiO/ceramic foam catalyst. *Int. J. Hydrogen Energy* **2015**, *40*, 7983−7990.

(9) Palm, M. O.; Silva Júnior, M. E.; Cardoso, L. R.; Duarte, D. A.; Catapan, R. C. On the Effect of the Washcoat on the Partial Oxidation and Steam Reforming of Ethanol on Ni/Al2O3Monolith in Short-Contact-Time Reactors. *Energy Fuels* **2020**, *34*, 2205−2213.

(10) Hou, T.; Zhang, S.; Chen, Y.; Wang, D.; Cai, W. Hydrogen production from ethanol reforming: catalysts and reaction mechanism. *Renewable Sustainable Energy Rev.* **2015**, *44*, 132−148.

(11) Kumar, A. Ethanol Decomposition and Dehydrogenation for Hydrogen Production: A Review of Heterogeneous Catalysts. *Ind. Eng. Chem. Res.* **2021**, *60*, 16561−16576.

(12) Bilal, M.; Jackson, S. D. Ethanol steam reforming over Rh and Pt catalysts: effect of temperature and catalyst deactivation. *Catal. Sci. Technol.* **2013**, *3*, 754−766.

(13) Kourtelesis, M.; Panagiotopoulou, P.; Verykios, X. Influence of structural parameters on the reaction of low temperature ethanol steam reforming over Pt/Al2O3 catalysts. *Catal. Today* **2015**, *258*, 247−255. Selected contributions in the field of heterogeneous catalysis and photocatalysis that were presented at the eighth International Conference on Environmental Catalysis (ICEC 2014).

(14) Denny, S. R.; Lin, Z.; Porter, W. N.; Artrith, N.; Chen, J. G. Machine learning prediction and experimental verification of Pt-modified nitride catalysts for ethanol reforming with reduced precious metal loading. *Appl. Catal., B* **2022**, *312*, 121380.

(15) Komiyama, M.; Merrill, R. P.; Harnsberger, H. Concentration profiles in impregnation of porous catalysts: Nickel on alumina. *J. Catal.* **1980**, *63*, 35−52.

(16) Mang, T.; Breitscheidel, B.; Polanek, P.; Knözinger, H. Adsorption of platinum complexes on silica and alumina: Preparation of non-uniform metal distributions within support pellets. *Appl. Catal., A* **1993**, *106*, 239−258.

(17) Zhang, Q.; Li, T.; Kameyama, H.; Wu, Q.; Ma, X.; Wu, Y. Pt structured catalysts prepared using a novel competitive impregnation method for the catalytic combustion of propionic acid. *Catal. Commun.* **2014**, *56*, 27−31.

(18) Zhang, Q.; Luan, H.; Li, T.; Wu, Y.; Ni, Y. Study on Pt-structured anodic alumina catalysts for catalytic combustion of toluene: Effects of competitive adsorbents and competitive impregnation methods. *Appl. Surf. Sci.* **2016**, *360*, 1066−1074.

(19) Sun, M.; Zhou, S.; Wang, S.; Song, C. Optimized Design Method for Pt/SiO2-Al2O3 with High NH3-SCO Activity and Thermal Stability. *ACS omega* **2022**, *7*, 3177−3184.

(20) Liu, Q.; Rzepka, P.; Frey, H.; Tripp, J.; Beck, A.; Artiglia, L.; Ranocchiari, M.; van Bokhoven, J. Sintering behavior of carbon-supported Pt nanoparticles and the effect of surface overcoating. *Mater. Today Nano* **2022**, *20*, 100273.

(21) Seynnaeve, B.; Lauwaert, J.; Vermeir, P.; Van Der Voort, P.; Verberckmoes, A. Model-based control of iron- and copper oxide particle distributions in porous gamma-Al2O3 microspheres through careful tuning of the interactions during impregnation. *Mater. Chem. Phys.* **2022**, *276*, 125428.

(22) Heise, M.; Schwarz, J. Preparation of metal distributions within catalyst supports. I. Effect of ph on catalytic metal profiles. *J. Colloid Interface Sci.* **1985**, *107*, 237−243.

(23) Greczynski, G.; Hultman, L. Reliable determination of chemical state in x-ray photoelectron spectroscopy based on sample-work-function referencing to adventitious carbon: resolving the myth of apparent constant binding energy of the C 1s peak. *Appl. Surf. Sci.* **2018**, *451*, 99−103.

(24) Kocemba, I.; Śmiechowicz, I.; Jędrzejczyk, M.; Rogowski, J.; Rynkowski, J. M. High Catalytic Activity of Pt/Al2O3 Catalyst in CO Oxidation at Room Temperature—A New Insight into Strong Metal−Support Interactions. *Catalysts* **2021**, *11*, 1475.

(25) Ono, L. K.; Yuan, B.; Heinrich, H.; Cuenya, B. R. Formation and thermal stability of platinum oxides on size-selected platinum nanoparticles: support effects. *J. Phys. Chem. C* **2010**, *114*, 22119−22133.

(26) Moulder, J.; Chastain, J. *Handbook of X-ray Photoelectron Spectroscopy: A Reference Book of Standard Spectra for Identification and Interpretation of XPS Data*; Physical Electronics Division, Perkin-Elmer Corporation, 1992.

(27) Vergunst, T.; Kapteijn, F.; Moulijn, J. A. Monolithic catalysts—Non-uniform active phase distribution by impregnation. *Appl. Catal., A* **2001**, *213*, 179−187.

(28) Shyr, Y.-S.; Ernst, W. R. Preparation of nonuniformly active catalysts. *J. Catal.* **1980**, *63*, 425−432.

(29) Chen, D.; Howe, K. J.; Dallman, J.; Letellier, B. C. Corrosion of aluminium in the aqueous chemical environment of a loss-of-coolant accident at a nuclear power plant. *Corros. Sci.* **2008**, *50*, 1046−1057.

(30) Liu, Q.; Qin, H.; Boscoboinik, J. A.; Zhou, G. Comparative study of the oxidation of NiAl (100) by molecular oxygen and water vapor using ambient-pressure X-ray photoelectron spectroscopy. *Langmuir* **2016**, *32*, 11414−11421.

(31) Li, W.; Sun, Z.; Tian, D.; Nevirkovets, I. P.; Dou, S.-X. Platinum dendritic nanoparticles with magnetic behavior. *J. Appl. Phys.* **2014**, *116*, 033911.

(32) Li, N.; Tang, S.; Meng, X. Preparation of Pt−GO composites with high-number-density Pt nanoparticles dispersed uniformly on GO nanosheets. *Prog. Nat. Sci.: Mater. Int.* **2016**, *26*, 139−144.

(33) Videla, A. H. A. M.; Osmieri, L.; Alipour Moghadam Esfahani, R.; Zeng, J.; Francia, C.; Specchia, S. The Use of C-MnO2 as Hybrid Precursor Support for a Pt/C-Mn x O1+ x Catalyst with Enhanced Activity for the Methanol Oxidation Reaction (MOR). *Catalysts* **2015**, *5*, 1399−1416.

(34) Ciambelli, P.; Palma, V.; Ruggiero, A. Low temperature catalytic steam reforming of ethanol. 2. Preliminary kinetic investigation of Pt/CeO2 catalysts. *Appl. Catal., B* **2010**, *96*, 190−197.

(35) Rahmani, F.; Haghighi, M.; Estifaee, P. Synthesis and characterization of Pt/Al2O3−CeO2 nanocatalyst used for toluene abatement from waste gas streams at low temperature: Conventional vs. plasma−ultrasound hybrid synthesis methods. *Microporous Mesoporous Mater.* **2014**, *185*, 213−223.

(36) Xu, D.; Li, W.; Duan, H.; Ge, Q.; Xu, H. Reaction performance and characterization of Co/Al2O3 Fischer−Tropsch catalysts promoted with Pt, Pd and Ru. *Catal. Lett.* **2005**, *102*, 229−235.

(37) Tengco, J. M. M.; Lugo-José, Y. K.; Monnier, J. R.; Regalbuto, J. R. Chemisorption−XRD particle size discrepancy of carbon supported palladium: Carbon decoration of Pd? *Catal. Today* **2015**, *246*, 9−14. Scientific Bases for the Preparation of Heterogeneous Catalysts Highlights of the 11th International Symposium Louvain-la-Neuve, Belgium, July 6−10, 2014.

(38) Bel'skaya, O. B.; Duplyakin, V. K. Molecular mechanism of formation of supported platinum catalysts of the Pt/Al2O3 family. *Russ. J. Gen. Chem.* **2007**, *77*, 2232−2242.

(39) Agrafiotis, C.; Tsetsekou, A. The effect of powder characteristics on washcoat quality. Part I: Alumina washcoats. *J. Eur. Ceram. Soc.* **2000**, *20*, 815−824.

(40) Simson, A.; Waterman, E.; Farrauto, R.; Castaldi, M. Kinetic and process study for ethanol reforming using a Rh/Pt washcoated monolith catalyst. *Appl. Catal., B* **2009**, *89*, 58−64.

(41) Salge, J.; Deluga, G.; Schmidt, L. Catalytic partial oxidation of ethanol over noble metal catalysts. *J. Catal.* **2005**, *235*, 69−78.

(42) Liguras, D. K.; Kondarides, D. I.; Verykios, X. E. Production of hydrogen for fuel cells by steam reforming of ethanol over supported noble metal catalysts. *Appl. Catal., B* **2003**, *43*, 345−354.

(43) Hung, C.-C.; Chen, S.-L.; Liao, Y.-K.; Chen, C.-H.; Wang, J.-H. Oxidative steam reforming of ethanol for hydrogen production on M/Al2O3. *Int. J. Hydrogen Energy* **2012**, *37*, 4955−4966. Optimization Approaches to Hydrogen Logistics.

(44) Mang, T.; Breitscheidel, B.; Polanek, P.; Knözinger, H. Adsorption of platinum complexes on silica and alumina: Preparation of non-uniform metal distributions within support pellets. *Appl. Catal., A* **1993**, *106*, 239−258.